Spring 2019

# Antitumor Properties of Imidazolium Salts

Jenna Frantz
jlf182@zips.uakron.edu

Jenna Frantz

Department of Biology
Honors Research Project
Fall and Spring semesters, 2018-2019

# Antitumor Properties of Imidazolium Salts

**Abstract:**

This is the final write-up for an honors research project for the University of Akron Williams Honors College. Synthesis of novel imidazolium salts was conducted. Following synthesis of imidazolium salts, the stability of the compound was tested at 37°C over a 72-hour period to give preliminary information about drug stability in vivo. 2D NMR was also conducted to confirm the structure of TPP-1. The student wrote an experimental protocol for the use of C57BL/6 mice and performed the online CITI training by the IRB to prepare to work with animals in a study of the antitumor properties of imidazolium salts in mice. Plausible physiological mechanisms by which the imidazolium cations exert their anti-tumor effects are discussed; current evidence demonstrates that imidazolium cations may be targeting the mitochondria of cancer cells.

**Introduction:**

Lung cancer is a deadly disease. The American Cancer Society predicts that about 230,000 new cases of lung cancer will develop and about 150,000 deaths will be caused by lung cancer in the United States in 2019 (American Cancer Society, 2019). Current medical treatments for lung cancer have low success rates (Thatcher et al., Sandler et al., Garon et al., Brahmer et al., Borghaei et al., Reck et al., Yang et al.), so it is important to perform studies to search for treatments that have higher success rates or increase length of overall survival after treatment. The problems associated with current cancer treatments include resistance to treatment, increased risk of infection, and side effects, such as nausea, vomiting, pain, neuropathy, hair loss, anemia, bleeding, and appetite loss (American Cancer Society, 2016). The data collected during this project will contribute to the development of new treatment options for

cancer, which could improve quality of life and save the lives of non-small cell lung cancer patients. Imidazolium salts are currently being researched for their potential antitumor properties.

In this project, a novel imidazolium salt (1,3-bis(naphthalen-2-ylmethyl)-2-phenyl-benzimidazolium bromide) was synthesized. We confirmed synthesis of this product with $^{1}H$ NMR and $^{13}C$ NMR. A stability study of TPP-1 (1,3-bis(naphthalen-2-ylmethyl)-2-(2-(triphenylphosphonio)ethyl)-benzoimidazolium dibromide) was also performed. This stability study consisted of $^{1}H$ NMR and $^{31}P$ NMR at time points 0, 2, 4, 8, 24, 48, and 72 hours to observe the degradation of this compound over time. The sample was held at 37°C throughout the course of the 72-hour study to mimic body temperature. 2D NMR was performed to confirm structure of TPP-1. We also address data from NCI-60 cell line panels for TPP-1 and IS-121 and discuss the efficacy of these two compounds in vitro. An in vivo study was proposed to test the antitumor properties of the novel imidazolium salt TPP-1 on C57BL/6 mice. An experimental protocol for the use of animals was written by the student, and the student performed CITI training for use of animals. A brief overview of the proposed in vivo study is discussed.

**Mechanism of antitumor activity of imidazolium salts:**

Imidazolium cations are of current interest in compounds with antitumor properties, because it has been shown that imidazolium cations target the mitochondria of cancer cells more than that of non-cancerous cells, leading to apoptosis in cancerous cells. The reason that imidazolium cations target cancer cells more than non-cancer cells is because cancer cells are more negatively-charged than non-cancer cells.

In all cells, the mitochondrial matrix is negatively charged because during oxidative phosphorylation, $H^{+}$ ions are pumped from the matrix into the intermembrane space, therefore

hyperpolarizing the matrix. Although $H^+$ will diffuse down their gradient from the intermembrane space into the matrix, which would have a depolarizing effect, the membrane does not actually become depolarized because $H^+$ are continually pumped up their gradient into the intermembrane space by the respiratory chain complexes; this maintains the inner mitochondrial membrane in a hyperpolarized state (Forrest, 2015).

The inner mitochondrial membrane of cancer cells is even more hyperpolarized than that of non-cancerous cells. This effect is especially exaggerated when the cancer cells are utilizing aerobic glycolysis. Because of the high rates of proliferation of cancer cells, these cells have high rates of aerobic glycolysis, and therefore, cancer cells have extreme hyperpolarization of the mitochondrial membrane potential. The mitochondrial membrane potential of cancerous cells is about -220 mV, in comparison with about -140 mV in non-cancerous cells (Forrest, 2015).

Because the inner mitochondrial membrane is negatively charged, delocalized lipophilic cations (such as imidazolium salts) can cross the cell membranes and are attracted to the negatively-charged mitochondrial matrix. As a result, an accumulation of delocalized lipophilic cations occurs in the matrix (Forrest, 2015). Because cancerous cells are more hyperpolarized than non-cancerous cells, delocalized lipophilic cations are more attracted to cancer cells than non-cancerous cells. According to Forrest in a 2015 article about charge differences in cancerous and noncancerous cells, "Using the Nernst equation, if the ΨIM of a cancer cell is 60 mV more hyperpolarised than that of a normal cell – which is within the range of observation [14, 18-19] – then a single charged [delocalized lipophilic cation] will accumulate 10 times more in the mitochondrial matrix of cancer cells than normal cells (T=300 K). Delocalized lipophilic cations with a double charge will accumulate 100 times more." Therefore, delocalized lipophilic cations are quite selective for cancerous cells. By selectively targeting cancerous cells, delocalized

lipophilic cations may be a cancer treatment that could reduce overall side effects due to decreasing damage in healthy cells.

If the inner mitochondrial membrane starts to depolarize, the voltage-sensitive permeability transition pore can be opened and allow for the entrance of pre-apoptotic agents that will lead to apoptotic cell death (Forrest, 2015). Delocalized lipophilic cations may combat cancer cells because the accumulation of these cationic compounds in the mitochondria reduce the mitochondrial membrane potential and depolarize the membrane, thereby inducing the generation of reactive oxygen species, inhibiting ATP production, and overall disrupting the progress of cancer cell proliferation (Battogtokh et al., 2018).

Cancer treatments that utilize delocalized lipophilic cations may be useful in combatting resistance to cancer treatments, which is a present problem with cancer treatments that target DNA. If a treatment targets a specific DNA sequence, the cancer cells can undergo mutations that will render the treatment unable to exert its effects on the DNA and its protein-coding abilities; therefore, DNA mutations can lead to resistance of cancer against DNA-targeting treatments (Forrest, 2015). Since delocalized lipophilic cation treatments target the strongly hyperpolarized mitochondria (rather than the DNA) to induce apoptosis, it seems that cancerous cells will be unable to develop resistance to this type of treatment.

To test whether imidazolium salts exert their anti-cancer effects via a mitochondrial disruption mechanism, Debord et al. (2017) performed a JC-1 assay. JC-1 is a cationic dye; as a result of the negatively-charged mitochondrial matrix, this cationic dye is prone to accumulate in the mitochondria. Accumulations of the dye (due to its attraction to the negatively-charged inner mitochondrial membrane) lead to a red color in the mitochondria and green in the cytosol. However, if the mitochondrial membrane potential is disrupted, aggregations of the dye do not

occur, and imaging therefore shows green with little to no red fluorescence; instead, only green fluorescence is observed (Debord et al., 2017). In cancerous cell lines, cells treated with imidazolium salts showed very little red fluorescence in the JC-1 assay, whereas the control (non-cancerous) cells showed the expected, non-disrupted red fluorescence in the mitochondria and green fluorescence in the cytosol (Debord et al., 2017). This suggests that the imidazolium salts had successfully disrupted the mitochondrial membrane potential of the cancerous cells, supporting the hypothesis that the mechanism of antitumor activity of imidazolium salts is by disruption of the hyperpolarized mitochondrial membrane potential.

**Synthesis of 2-phenylbenzimidazole and 1,3-bis(naphthalen-2-ylmethyl)-2-phenyl-benzimidazolium bromide**

The synthesis of our product consisted of multiple steps. First, 2-phenylbenzimidazole was synthesized (Figure 1), and NMR was utilized to confirm synthesis (Figure 2). Once formation of this product was verified, we continued our reaction to add on substituents and synthesize 1,3-bis(naphthalen-2-ylmethyl)-2-phenylbenzimidazolium bromide (Figure 3). Again, we confirmed synthesis with NMR (Figure 4, Figure 5).

*Synthesis of 2-phenyl-benzimidazole:*

To synthesize 2-phenyl-benzimidazole, 0.998 grams of o-phenylenediamine, 945 μL of benzaldehyde, and 10 mL dry DMF were placed into a 50 mL round bottom flask. The mixture was heated to 145ºC and stirred for 12 hours. The reaction was poured into a 50 mL Erlenmeyer flask, and a yellow precipitate formed. The precipitate was collected via vacuum filtration. The product was washed with ether and collected via vacuum filtration, which yielded 1.015 grams of pale, yellow solid. This was a 56% yield.

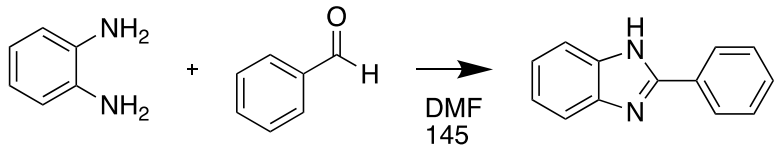


Figure 1. Synthesis of 2-phenyl-benzimidazole

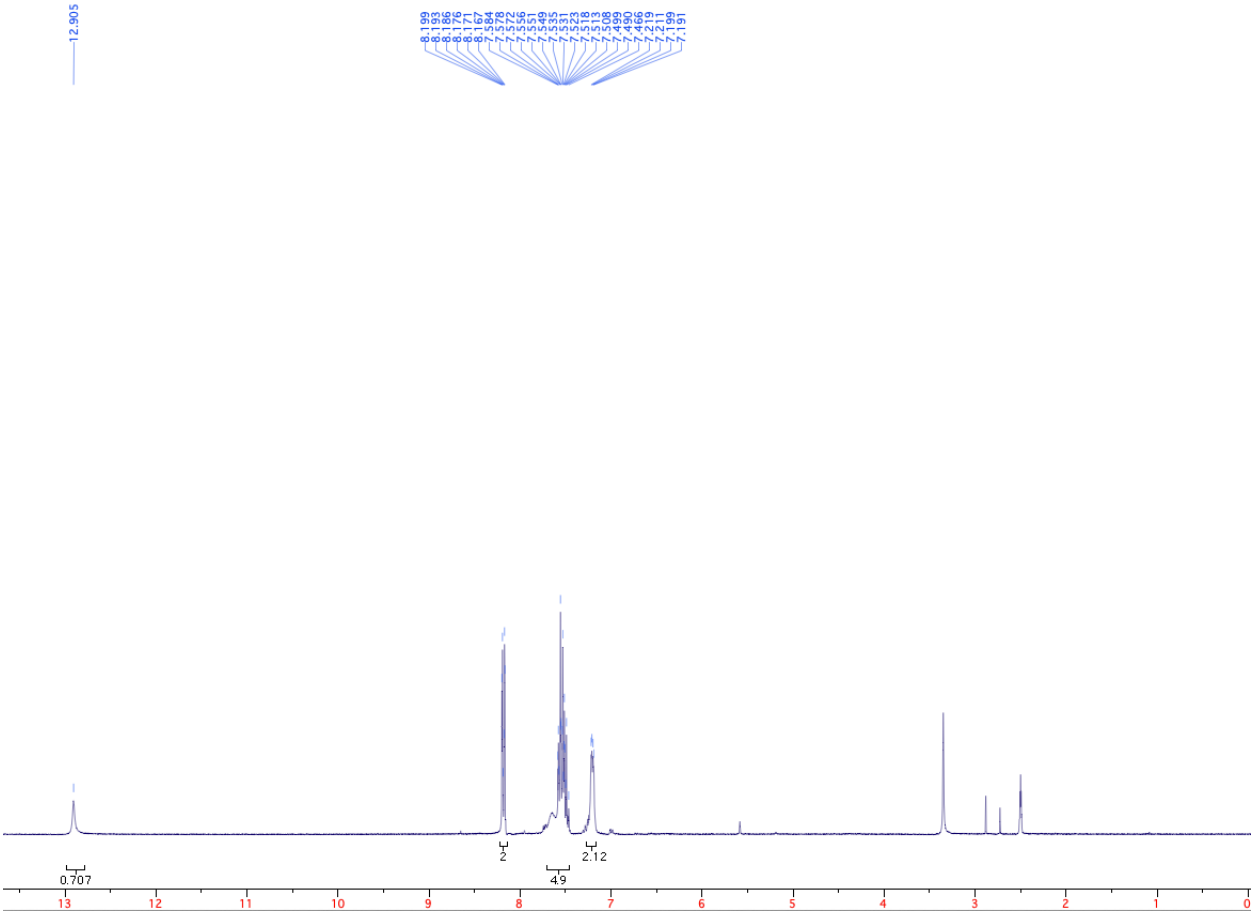


Figure 2. 2-phenylbenzimidazole $^{1}$H-NMR (300 MHz; DMSO-$d_6$): δ 12.91 (s, 1H), 8.20-8.17 (m, 2H), 7.58-7.47 (m, 5H), 7.20 (dd, $J$ = 6.0, 2.3 Hz, 2H).

*Synthesis of 1,3-bis(naphthalen-2-ylmethyl)-2-phenyl-benzimidazolium bromide:*

For the synthesis of 1,3-bis(naphthalen-2-ylmethyl)-2-phenyl-benzimidazolium bromide, 1.015 g of 2-phenyl-benzimidazole from the previous reaction, 350 mg KOH, and 10 mL dry acetonitrile were put into a 50 mL round bottom flask and heated at reflux with stirring for 30 minutes. After this period of reflux with stirring, 1.19 g of 2-(bromomethyl)-naphthalene was added and heated at reflux with stirring for 24 hours. The solution was filtered hot to remove KBr and volatiles were removed to give an orange oil. NMR showed a mono-substituted product. After confirming synthesis of the mono-substituted product, we added 1.19 g of 2-(bromomethyl)-naphthalene and 10 mL dry acetonitrile to the reaction mixture and heated to reflux with stirring for about 16 hours. Volatiles were removed, the product was recrystallized in ethanol, and the product was collected by vacuum filtration. The solid was washed with ether and collected by vacuum filtration to give 1.43 g of white solid, which was a 49% yield.

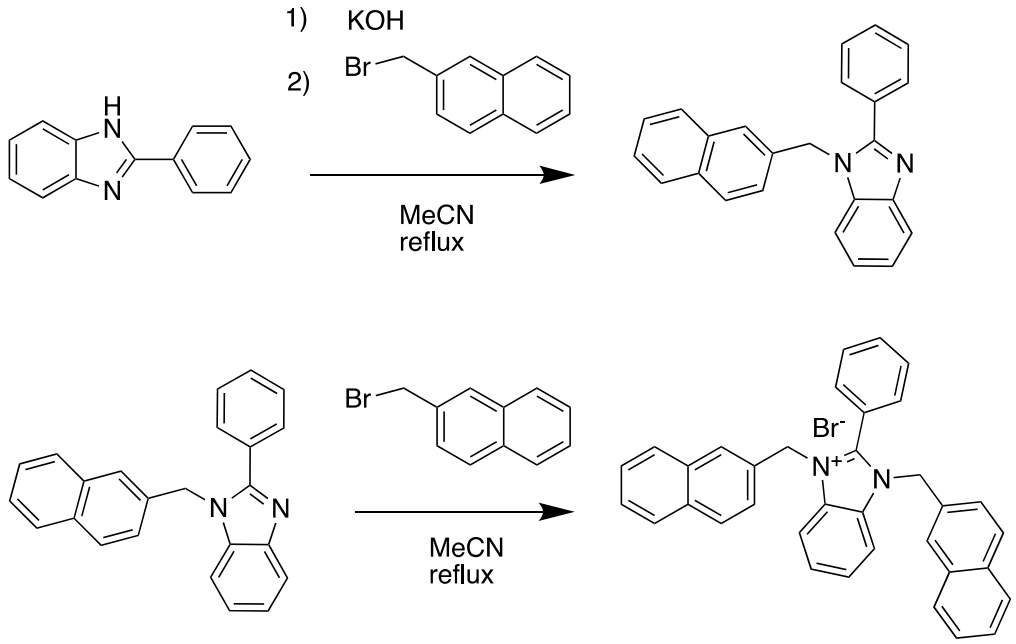


Figure 3. Synthesis of 1,3-bis(naphthalen-2-ylmethyl)-2-phenyl-benzimidazolium bromide

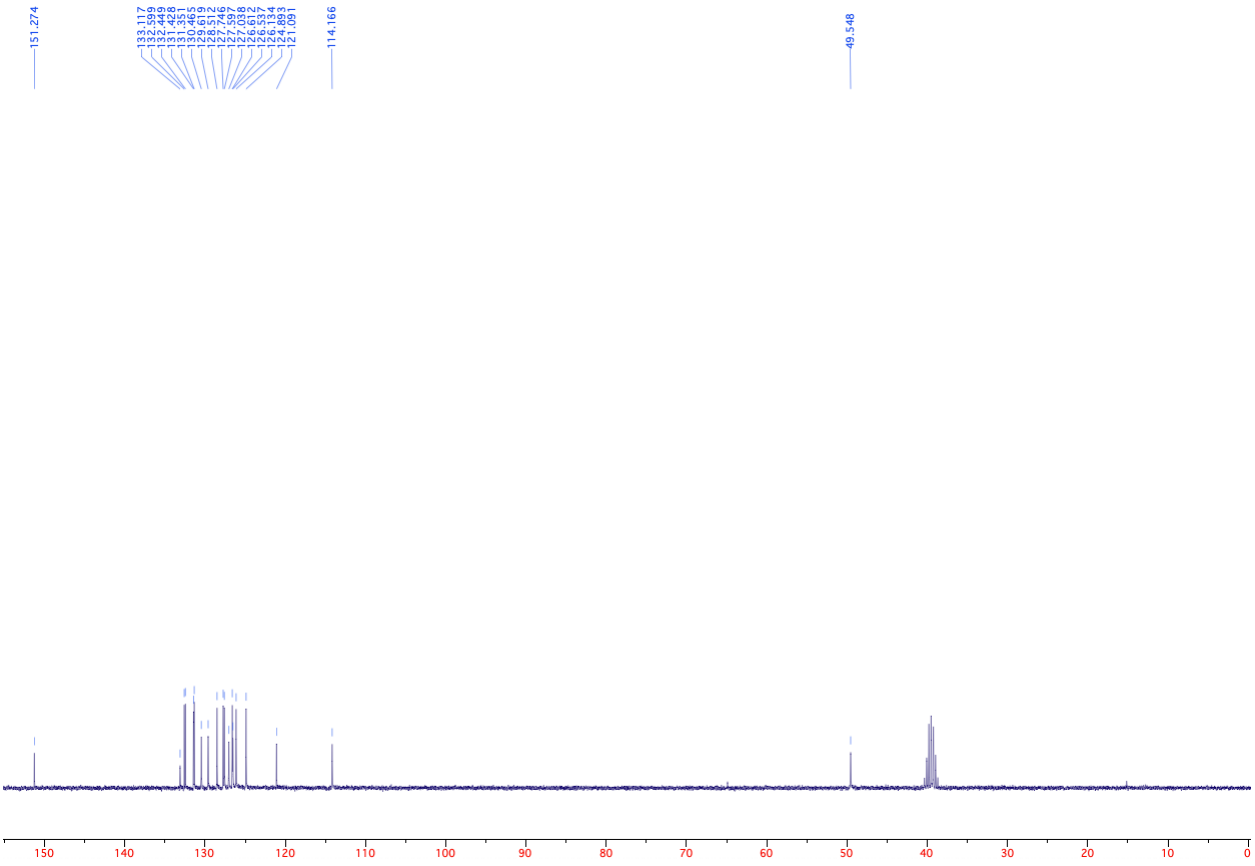


Figure 4. 1,3-bis(naphthalen-2-ylmethyl)-2-phenyl-benzimidazolium bromide $^{13}$C-NMR (300 MHz; DMSO-$d_6$)

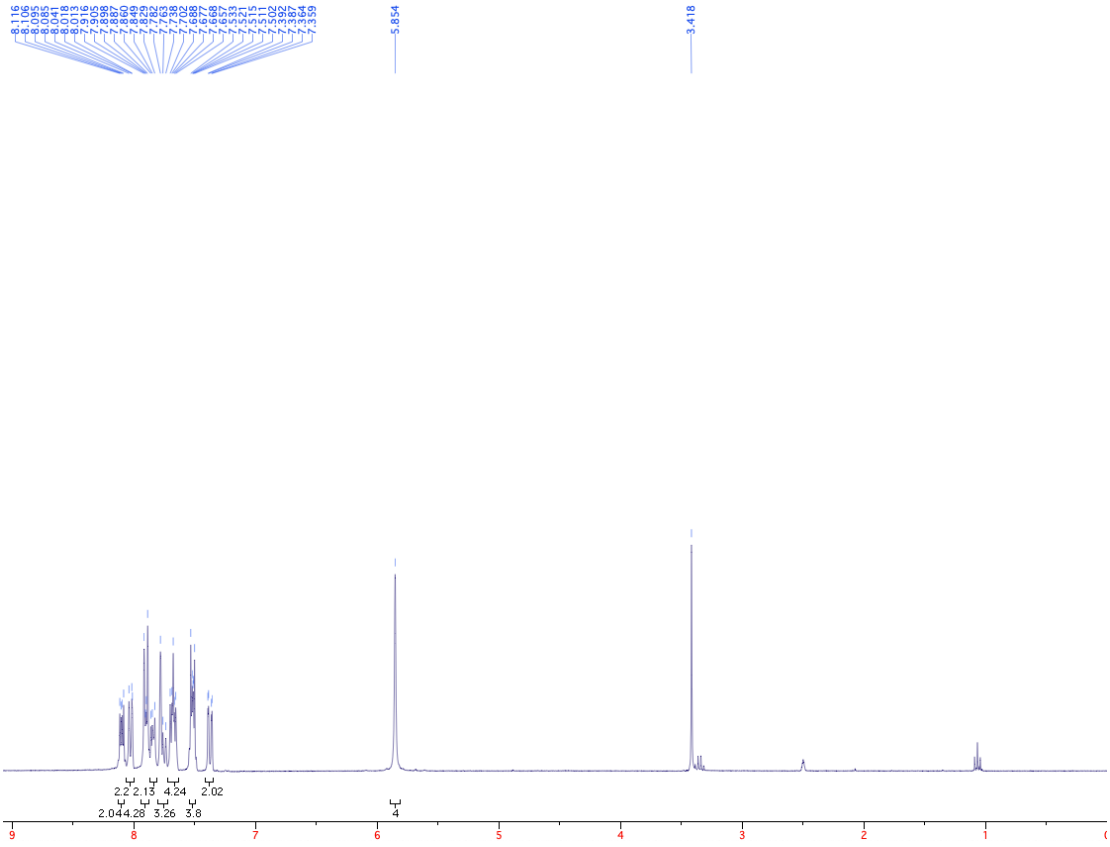


Figure 5. 1,3-bis(naphthalen-2-ylmethyl)-2-phenyl-benzimidazolium bromide $^{1}$H-NMR (300 MHz; DMSO-$d_6$): δ 8.10 (dd, $J$ = 6.3, 3.1 Hz, 2H), 8.04-8.01 (m, 2H), 7.92-7.89 (m, 4H), 7.86-7.83 (m, 2H), 7.78-7.74 (m, 3H), 7.68 (dt, $J$ = 6.5, 3.4 Hz, 4H), 7.53-7.50 (m, 4H), 7.38 (dd, $J$ = 8.5, 1.6 Hz, 2H), 5.85 (s, 4H).

**Stability Study of TPP-1**

The stability of the imidazolium salt TPP-1 was studied over a period of 3 days. To prepare the sample for NMR studies, 10 mg of TPP-1 was dissolved in a solution of 50% DMSO $d_6$ / $D_2O$ (350 µL DMSO in 350 µL $D_2O$).

$^{1}$H and $^{31}$P NMR were obtained (Figure 6, Figure 7). The NMR of the sample was collected at time points 0, 2, 4, 8, 24, 48, and 72 hours. The sample was heated in the NMR

warmer at 37°C to mimic body temperature.  A thermometer was placed into one of the slots of the NMR warmer to confirm temperature.

Before putting a compound into an animal or human body, it is important to understand how it will be absorbed, distributed in the body (which organs it goes to), metabolism of the compound, and elimination (how it is cleared from the body). The stability study was performed as part of understanding drug stability in the animal; therefore, the sample of TPP-1 was held at 37ºC to mimic body temperature. NMR was taken at time points 0, 2, 4, 8, 24, 48, and 72 hours in order to provide a preliminary look at how this product may break down over time in the body.

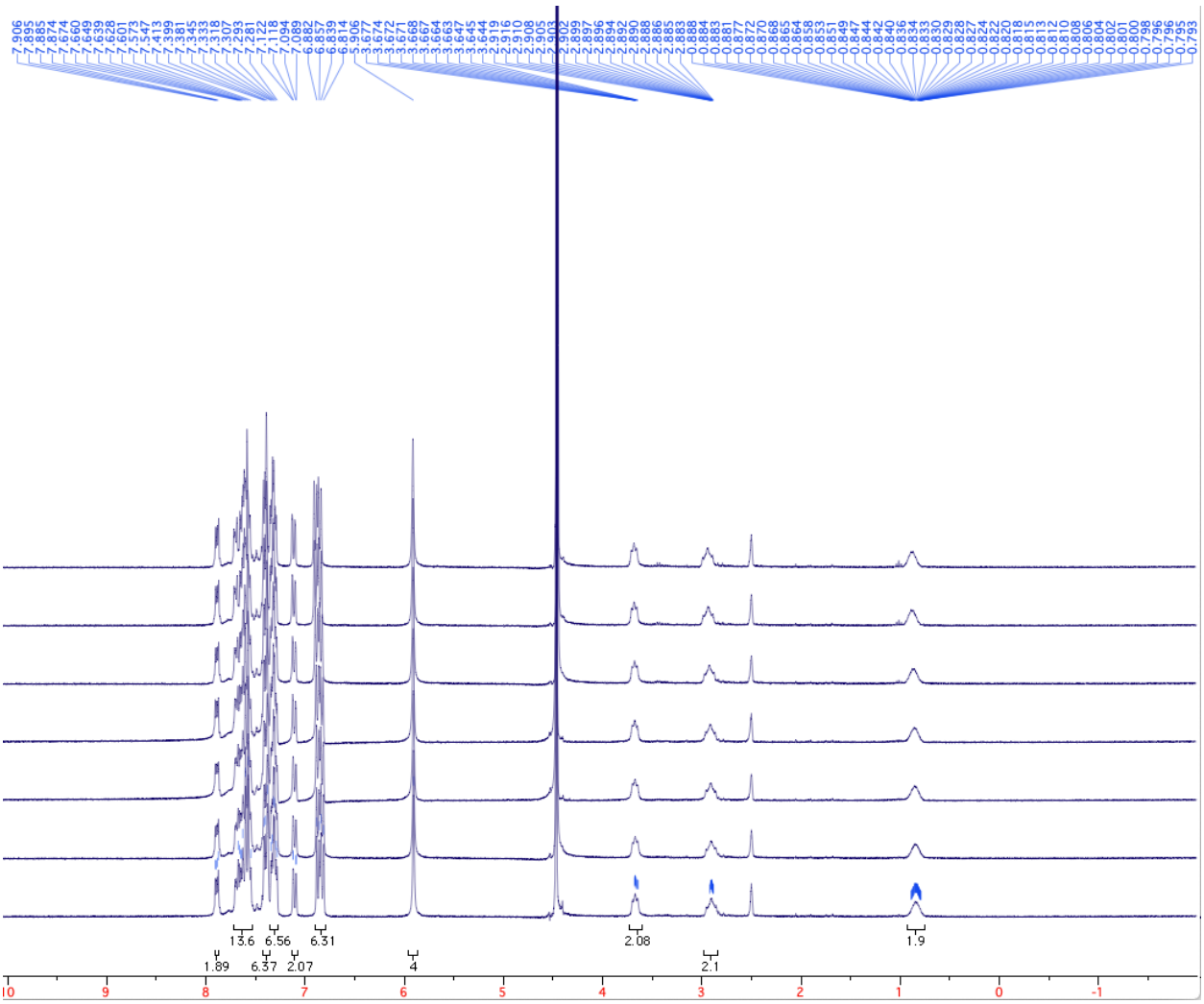


Figure 6. TPP-1 $^{1}$H-NMR (300 MHz; DMSO-d$_6$) at 0, 2, 4, 8, 24, 48, and 72 hours: δ 7.89 (dd, *J* = 6.3, 3.1 Hz, 2H), 7.67-7.55 (m, 14H), 7.41-7.38 (m, 6H), 7.31 (td, *J* = 7.9, 3.5 Hz, 7H), 7.11 (dd, *J* = 8.6, 1.3 Hz, 2H), 6.85 (dd, *J* = 12.9, 7.5 Hz, 6H), 5.91 (s, 4H), 3.68-3.64 (m, 2H), 2.92-2.88 (m, 2H), 0.89-0.79 (m, 2H).

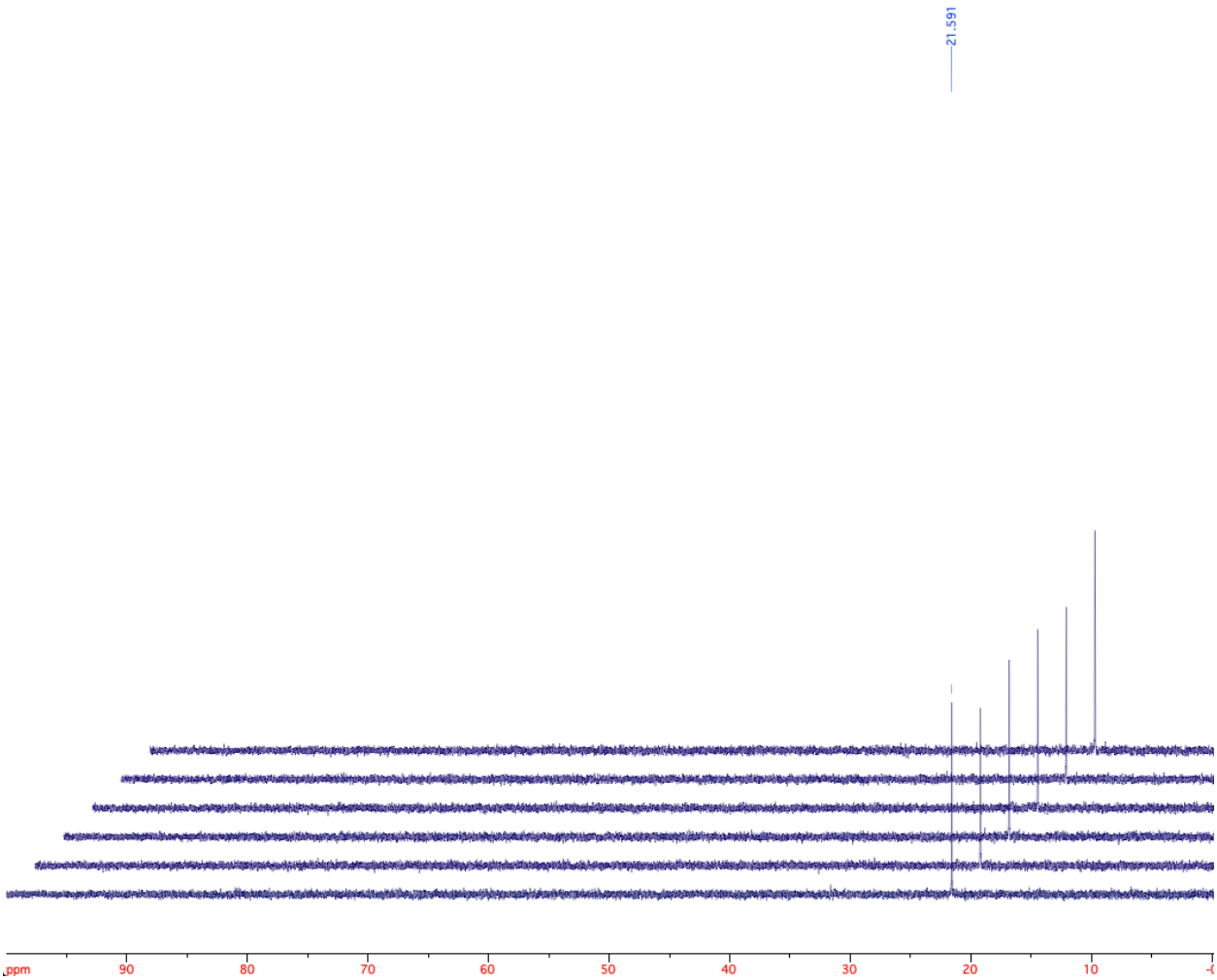


Figure 7. TPP-1 $^{31}$P-NMR (300 MHz; DMSO-$d_6$) at 0, 2, 4, 8, 24, 48, and 72 hours.

**2D NMR Experiments**

A COSY 2D NMR spectrum was obtained to further confirm the structure of TPP-1 (Figure 8). COSY 2D NMR correlates the protons to one another through one bond coupling. The COSY spectrum of TPP-1 does not offer much detail other than the coupling of the alkyl protons at 4.02, 3.97, and 1.90 ppm (Figure 9). The proton resonances at 4.02 and 3.97 are too close together to determine significant coupling. This data does show that the alkyl protons

around 4 ppm are coupled to the multiplet at 1.90 ppm (Figure 9). The resonance at 1.90 ppm was presumed to be the middle alkyl in the propanol chain.

Since the COSY NMR did not provide much information about the structure of TPP-1, an HSQC 2D NMR ($^{1}H - {}^{13}C$) was obtained (Figure 10). The results of this experiment were used to determine that the alkyl closest to the phosphorous was the multiplet at 3.97 ppm in the $^{1}H$ NMR which correlated to the resonance at 20.1 ppm (Figure 10). In addition, a strange phenomenon was observed with the alkyl in the middle of the propyl chain. This resonance was largely split due to coupling to phosphorus in the $^{1}H$ NMR, but in the $^{13}C$ little splitting was observed. Additionally, the resonance for the carbon and protons directly bound by to the imidazole nitrogen were also contradicting one another. The resonance in the $^{1}H$ NMR at 4.02 ppm was a slightly broadened triplet, but in the $^{13}C$ a doublet carbon resonance at 24.2 ppm was shown to be correlating to this signal (Figure 10). We were unable to explain this result. In addition to the alkyl data, the HSQC experiment also provided important information about the aromatic carbon resonances. Although the $^{1}H$ NMR showed less discernable structural data, all carbon aromatic resonances with an attached proton were assigned when $^{1}H$ NMR data was combined with $^{13}C$ NMR. Commonly, the carbon resonance directly bound to phosphorus appears at 118 ppm with a large J-coupling (Kaiser, et al. 2006). The aromatic carbon bound directly to phosphorus was suspected to be at 117.6 ppm with a J-coupling of 86 Hz, because it was the only resonances at the lower aromatic range with no protons correlated to the signal.

In addition, another HSQC experiment was conducted to determine the correlation between $^{1}H$ and $^{31}P$ (Figure 11). The interactions of protons to other nuclei in an HSQC experiment are commonly one-bond coupling, but due to the larger coupling constants of $^{1}H - {}^{31}P$, some two-bond coupling was observed. The correlation experiment was used to determine

which protons were directly adjacent to the phosphorus atom. It was determined that the proton resonance at 3.97 ppm was adjacent to the phosphorus and bonded to the carbon signal at 20.1 ppm (Figure 11). Furthermore, the aromatic protons that were two bonds away from the phosphorus were also observed, but little structural information was provided other than the aromatic protons of TPP-1 were at the large multiplet at 7.54 ppm (Figure 11). Moreover, when the peak intensity of the 2-D spectrum was increased, the weak two bond coupling signal of the alkyl protons at 1.90 ppm was observed (Figure 11). This confirmed the alkyl resonances at 3.97 ppm (20.1 ppm) and 1.90 ppm (24.2 ppm) are bound one and two bonds away from the phosphorus, respectively.

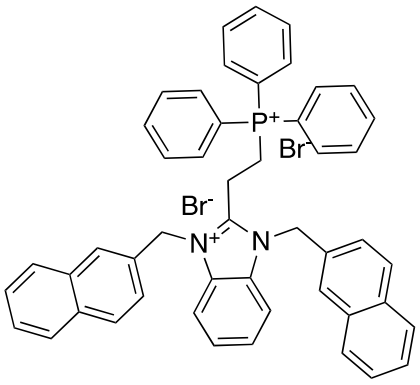


Figure 8. Structure of TPP-1

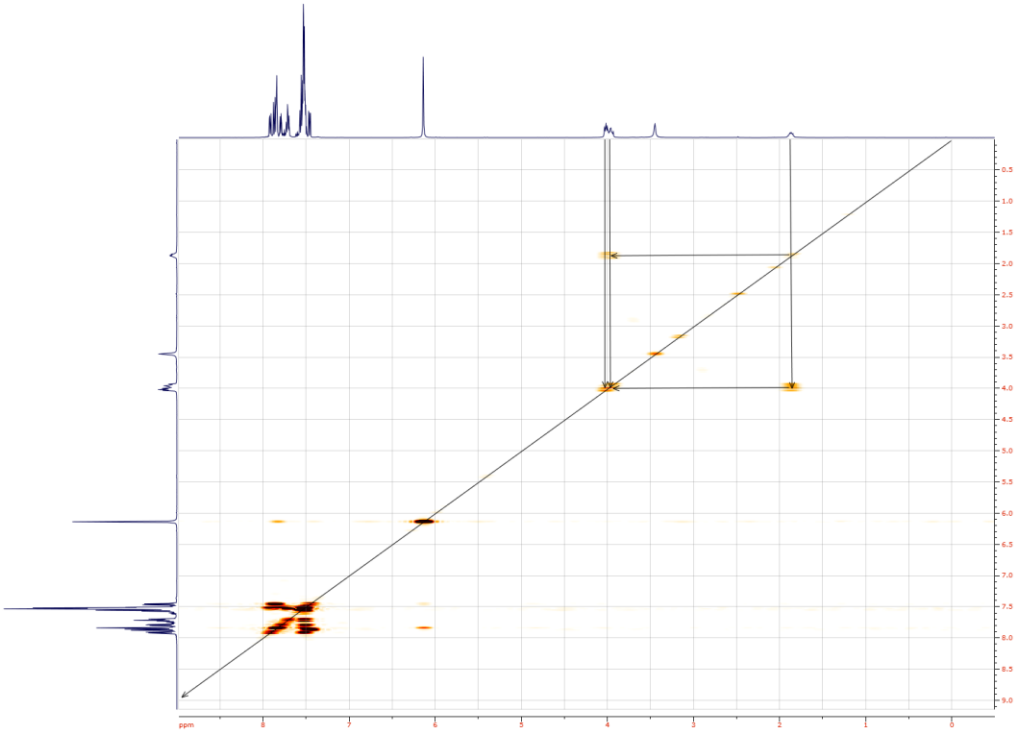

Figure 9. TPP-1 COSY $^{1}H$ – $^{1}H$

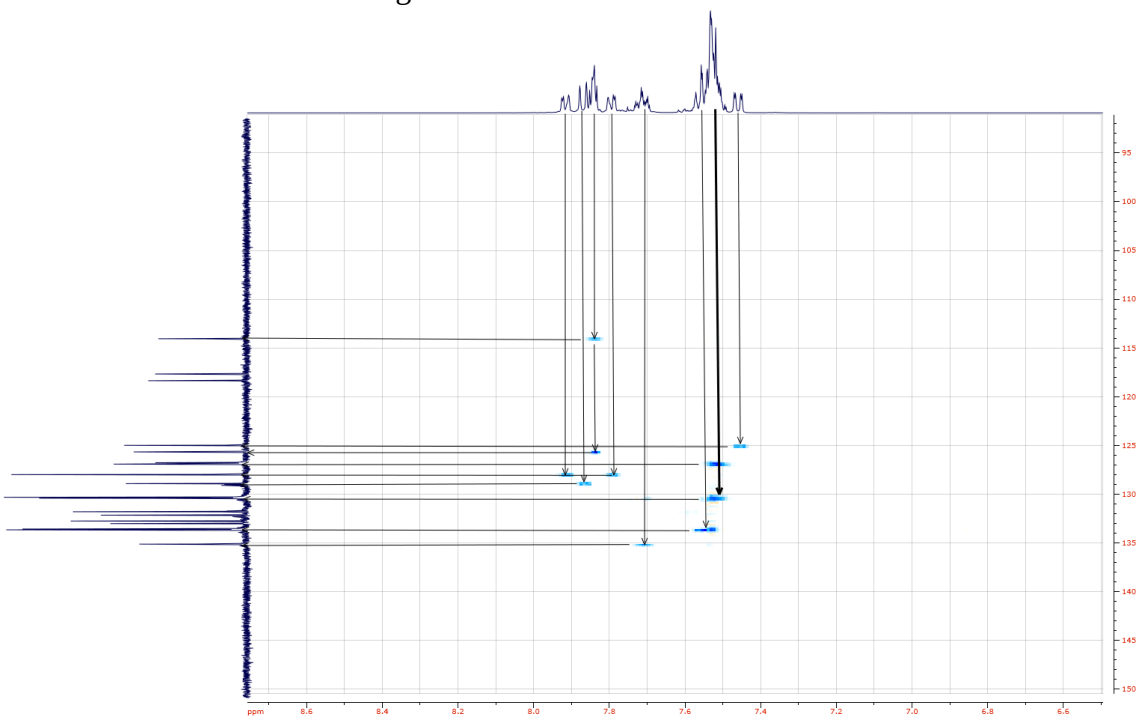

Figure 10. HSQC $^{13}C$ – $^{1}H$

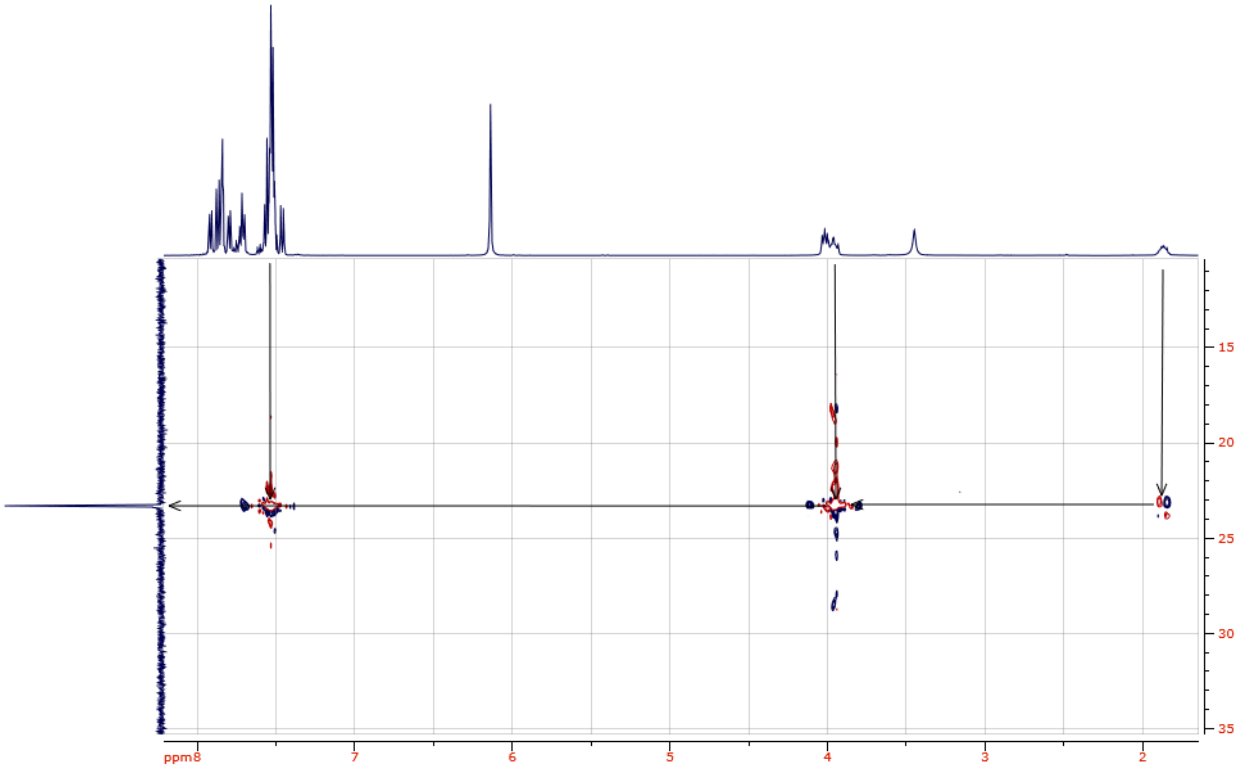


Figure 11. HSQC $^{31}P$ – $^{1}H$

**One-Dose Mean Graphs**

To interpret a one-dose mean graph, it is important to understand the meaning of the values in the graph. The value for growth rate is a comparison to the no-drug control. A 100% growth rate means that the experimental cell line experiences no inhibition relative to no-drug control. A cell line that has a 75% growth rate compared to control experiences 25% growth inhibition. A cell line that experiences a -75% growth rate experiences 75% lethality. A growth rate of -100% means that there was 100% lethality and all cells are dead.

Cell lines treated with TPP-1 experienced a mean of 55.99% growth relative to the no-drug control (Figure 12), whereas cell lines treated with IS-121 had a mean growth of 13.71%

relative to the no-drug control (Figure 13). This means that cell lines treated with TPP-1 had a mean of 44.01% growth inhibition, whereas cell lines treated with IS-121 experienced a mean of 86.29% growth inhibition.

Specifically for non-small cell lung cancer cell lines treated with TPP-1, results showed 34.82%-83.54% growth rates relative to control, with a mean of 59.33% (i.e. range of 16.46%-65.18% growth inhibition, mean 40.67% growth inhibition; Figure 12). NSCLC cell lines treated with IS-121 exhibited a range of -24.30%-68.38% growth rate and a mean growth rate of 29.45% relative to control (31.62% inhibition to 24.30% lethality, with a mean of 70.55% growth inhibition; Figure 13). These results demonstrate that IS-121 is more effective at causing inhibition and lethality of NSCLC than TPP-1.

These findings are summarized in table 1 and figures 12 and 13, below.

| | Mean growth rate relative to control | Range of mean growth rate relative to control | Mean growth inhibition | Range of mean inhibition |
|---|---|---|---|---|
| TPP-1, all cell lines | 55.99% | 6.90%-100.09% | 44.01% | .09% growth-93.1% inhibition |
| IS-121, all cell lines | 13.71% | (-97.80%)-86.37% | 86.29% | 13.63% inhibition to 97.80% lethality |
| TPP-1, NSCLC | 59.33% | 34.82%-83.54% | 40.67% | 16.46%-65.18% |
| IS-121, NSCLC | 29.45% | (-24.30%)-68.38% | 70.55% | 31.62% inhibition to 24.30% lethality |

Table 1. Growth rate and growth inhibition of cell lines treated with TPP-1 and IS-121. Adapted from Developmental Therapeutics Program. Apr. 25, 2016 and Feb. 11, 2019. American Cancer Institute.

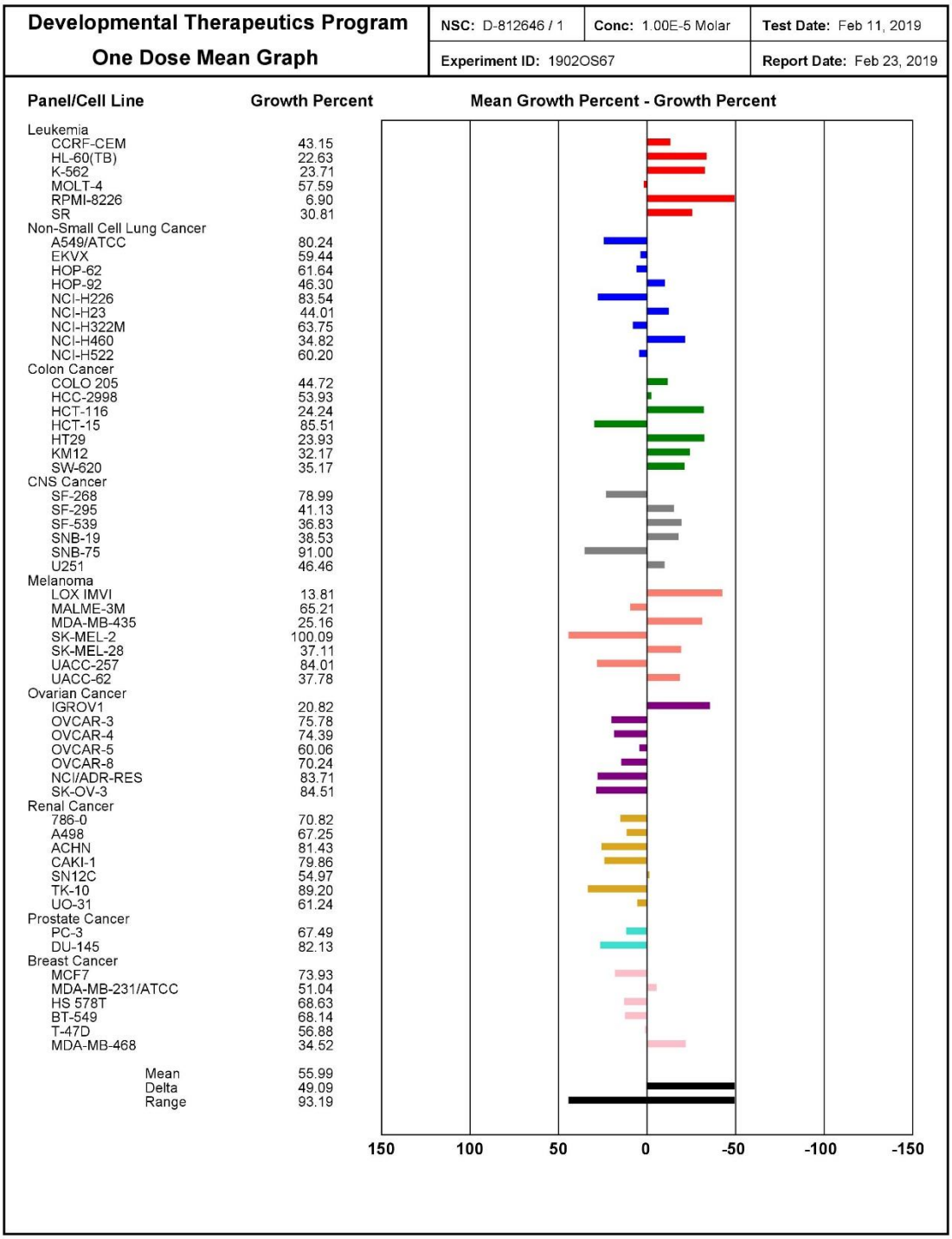


Figure 12. One Dose Mean Graph for TPP-1. Reprinted from Developmental Therapeutics Program. Feb. 11, 2019. American Cancer Institute.

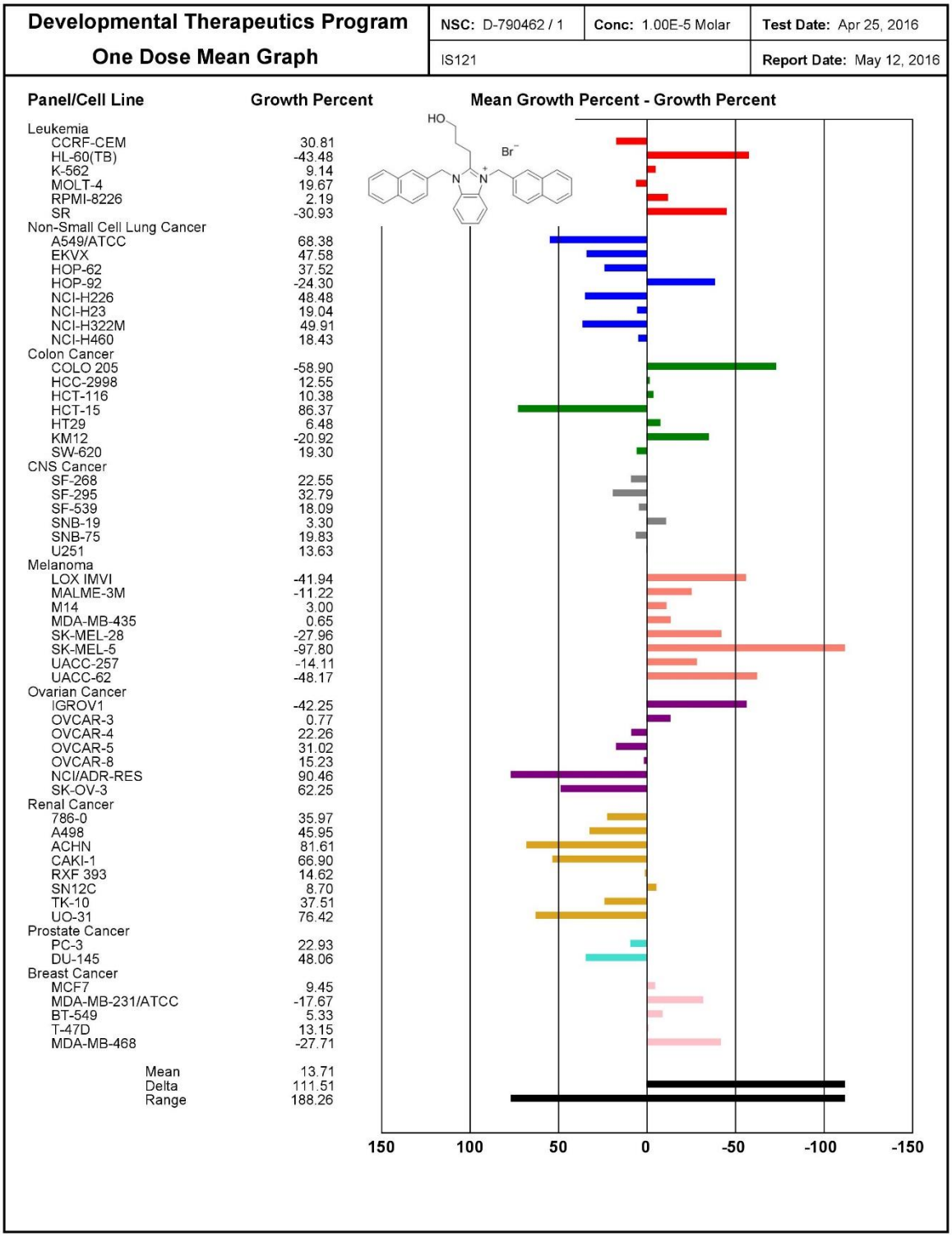


Figure 13. One Dose Mean Graph for IS-121. Reprinted from Developmental Therapeutics Program. Apr. 25, 2019. American Cancer Institute.

**In vivo study concept in C57BL/6 mice**

*Materials and methods:*

A protocol was written and CITI training from the IRB was performed by the student to be able to perform experiments with C57BL/6 mice. We planned to use TPP-1 as our experimental treatment against non-small cell lung cancer (NSCLC) in C57BL/6 mice, but the results from NCI-60 cell line screen in February 2019 by the Developmental Therapeutics showed that TPP-1 is not as effective at inhibiting cancer cell growth or causing lethality as other compounds (Figure 12, Figure 13). The compound IS-121 has produced results for the one-dose mean graph that show that IS-121 has stronger properties of inhibition and lethality in cancer cell lines (Figure 2). Therefore, it was deemed inhumane and unethical to use TPP-1 in experimental studies using animals due to the undue harm and suffering they would undergo for testing of a compound with only meager anti-tumor properties in comparison with other compounds. The plan for the in vivo experiments in C57BL/6 mice is described in detail below because of its future applications; other antitumor compounds could be tested using the procedures described below.

According to the protocol written by the student, the in vivo experiment would consist of an experimental group of C57 BL/6 mice, which receives the imidazolium salt treatment, and a control group of C57 BL/6 mice, which receives a placebo saline solution. The C57BL/6 mice would receive Lewis Lung Carcinoma (LLC) cells via subcutaneous injection on the back (Kellar, et al., 2015). Tumor growth would be monitored for 2 weeks. The tumor would be excised at 14 days, which consistently leads to metastasis (Gómez-Cuadrado, 2017). After tumor excision, the experimental and control groups would begin receiving their respective treatments and would receive these treatments for 2 weeks. During this time, the size of the tumors would

be measured with calipers. After the period of 2 weeks of treatment, during which the mice receive the imidazolium salt treatment or saline solution, the mice would be euthanized and tumor size and weight, as well as lung histology, would be measured.

**Discussion and Conclusion:**

The qualities of interest in a novel compound that may be used as a drug are synthesis, stability, efficacy, and ADME (absorption, distribution, metabolism, and excretion). To confirm synthesis, we performed NMR of 2-phenylbenzimidazole and 1,3-bis(naphthalen-2-ylmethyl)-2-phenyl-benzimidazolium bromide. The novel imidazolium salt synthesized in this study **(**1,3-bis(naphthalen-2-ylmethyl)-2-phenyl-benzimidazolium bromide) has not yet been tested for its potential antitumor properties. In the future, this compound could be tested in an NCI-60 cell line panel to test for potential antitumor activity.

Before putting a compound into an animal or human body, it is important to understand ADME: how it will be absorbed, where it will be distributed in the body (which organs it goes to), metabolism of the compound, and elimination (how it is cleared from the body). The stability study was performed as part of understanding drug stability in the animal; therefore, the sample of TPP-1 was held at 37°C to mimic body temperature. NMR was taken at time points 0, 2, 4, 8, 24, 48, and 72 hours to provide a preliminary look at how this product may break down over time in the body, which relates to how the body may metabolize and eliminate this compound.

TPP-1 compound was believed to have impressive tumor-targeting effects due to its double positive charge, but the NCI-60 cell line panels showed that TPP-1 is not as effective as IS-121 in inhibiting cancer cell growth. The reasons for the lack of efficacy of TPP-1 are not well understood and should be explored.

The in vivo study plan proposed by the student has future applications in that it could be utilized as a study model for other imidazolium cations to test for their antitumor properties in non-small cell lung cancer in C57BL/6 mice.

**Acknowledgements:**

I would like to thank Jason Bonezzi and Michael Stromyer for their invaluable assistance, generous help, and great teaching skills. I would also like to thank Dr. Youngs for his help in planning and coordinating my research, Dr. Paruchuri and Dr. Teegala for their assistance with the animal protocol, and Dr. Tessier for ensuring the quality of my honors research project.

**Resources:**

American Cancer Society. (2016, May 16). Chemotherapy for Non-Small Cell Lung Cancer. Retrieved April 5, 2019, from https://www.cancer.org/cancer/non-small-cell-lung-cancer/treating/chemotherapy.html

American Cancer Society. (2019, January 9). Key Statistics for Lung Cancer. Retrieved April 5, 2019, from https://www.cancer.org/cancer/non-small-cell-lung-cancer/about/key-statistics.html

Battogtokh, G., Choi, Y. S., Kang, D. S., Park, S. J., Shim, M. S., Huh, K. M., . . . Kang, H. C. (2018). Mitochondria-targeting drug conjugates for cytotoxic, anti-oxidizing and sensing purposes: Current strategies and future perspectives. *Acta Pharmaceutica Sinica B,8*(6), 862-880. doi:10.1016/j.apsb.2018.05.006

Borghaei H, Paz-Ares L, Horn L, et al. Nivolumab versus Docetaxel in Advanced Nonsquamous Non-Small-Cell Lung Cancer. N Engl J Med 2015;373:1627-39.

Brahmer J, Reckamp KL, Baas P, et al. Nivolumab versus Docetaxel in Advanced Squamous-Cell Non-Small-Cell Lung Cancer. N Engl J Med 2015;373:123-35.

Debord, M. A., Southerland, M. R., Wagers, P. O., Tiemann, K. M., Robishaw, N. K., Whiddon, K. T., . . . Youngs, W. J. (2017). Synthesis, characterization, in vitro SAR and in vivo evaluation of N,N′bisnaphthylmethyl 2-alkyl substituted imidazolium salts against NSCLC. *Bioorganic & Medicinal Chemistry Letters,27*(4), 764-775. doi:10.1016/j.bmcl.2017.01.035

Forrest, M. D. (2015). Why cancer cells have a more hyperpolarised mitochondrial membrane potential and emergent prospects for therapy. doi:10.1101/025197

Garon EB, Ciuleanu TE, Arrieta O, et al. Ramucirumab plus docetaxel versus placebo plus docetaxel for second-line treatment of stage IV non-small-cell lung cancer after disease progression on platinum-based therapy (REVEL): a multicentre, double-blind, randomised phase 3 trial. Lancet 2014;384:665-73.

Gómez-Cuadrado, L., Tracey, N., Ma, R., Qian, B., & Brunton, V. G. (2017). Mouse models of metastasis: progress and prospects. Disease models & mechanisms, 10(9), 1061–1074. doi:10.1242/dmm.030403

Kaiser, S.; Smidt, S. P.; Pfaltz, A. Iridium Catalysts with Bicyclic Pyridine-Phosphinite Ligands: Asymmetric Hydrogenation of Olefins and Furan Derivatives. *Angew. Chemie - Int. Ed.* 2006, *45*, 5194–5197.

Kellar, A., Egan, C., & Morris, D. (2015). Preclinical Murine Models for Lung Cancer: Clinical Trial Applications. BioMed Research International, 2015, 1-17. doi:10.1155/2015/621324

Lavon, H. et al. Dexmedetomidine promotes metastasis in rodent models of breast, lung, and colon cancers. British Journal of Anaesthesia. Volume 120, Issue 1, pp. 188-196.

One Dose Mean Graph for IS-121. Reprinted from Developmental Therapeutics Program. Apr. 25, 2019. American Cancer Institute.

One Dose Mean Graph for TPP-1. Reprinted from Developmental Therapeutics Program. Feb. 11, 2019. American Cancer Institute.

Pirker R, Pereira JR, Szczesna A, et al. Cetuximab plus chemotherapy in patients with advanced non-small-cell lung cancer (FLEX): an open-label randomised phase III trial. Lancet 2009;373:1525-31.

Reck M, Kaiser R, Mellemgaard A, et al. Docetaxel plus nintedanib versus docetaxel plus placebo in patients with previously treated non-small-cell lung cancer (LUME-Lung 1): a phase 3, double-blind, randomised controlled trial. Lancet Oncol 2014;15:143-55.

Sandler A, Gray R, Perry MC, et al. Paclitaxel-carboplatin alone or with bevacizumab for non-small-cell lung cancer. N Engl J Med 2006;355:2542-50.

Thatcher N, Hirsch FR, Luft AV, et al. Necitumumab plus gemcitabine and cisplatin versus gemcitabine and cisplatin alone as first-line therapy in patients with stage IV squamous non-small-cell lung cancer (SQUIRE): an open-label, randomised, controlled phase 3 trial. Lancet Oncol 2015;16:763-74.

Wright, B.D., Deblock, M.C., Wagers, P.O., Duah, E., Robishaw, N.K., Shelton, K.L., . . .Youngs, W. J. Anti-tumor activity of lipophilic imidazolium salts on select NSCLC cell lines. Medicinal Chemistry Research (2015), Medicinal Chemistry Research (2015), 24(7), 2838-2861.

Yang JC, Wu YL, Schuler M, et al. Afatinib versus cisplatin-based chemotherapy for EGFR mutation-positive lung adenocarcinoma (LUX-Lung 3 and LUX-Lung 6): analysis of overall survival data from two randomised, phase 3 trials. Lancet Oncol 2015;16:141-51.